

Contract No. DE-AC21-94MC31160--34

**PARTICULATE HOT GAS STREAM CLEANUP
TECHNICAL ISSUES**

Task 1 ASSESSMENT OF ASH CHARACTERISTICS

FINAL REPORT

October 1994 - September 1999

including the

QUARTERLY REPORT

July 1999 - September 1999

and the

ANNUAL REPORT

October 1998 - September 1999

Prepared for

UNITED STATES DEPARTMENT OF ENERGY
Federal Energy Technology Center - Morgantown
Post Office Box 880, 3610 Collins Ferry Road
Morgantown, West Virginia 26505

**PARTICULATE HOT GAS STREAM CLEANUP
TECHNICAL ISSUES**

Task 1 ASSESSMENT OF ASH CHARACTERISTICS

FINAL REPORT

October 1994 - September 1999

including the

QUARTERLY REPORT

July 1999 - September 1999

and the

ANNUAL REPORT

October 1998 - September 1999

SRI-ENV-99-8484-T1F

September 30, 1999

SOUTHERN RESEARCH INSTITUTE
2000 NINTH AVENUE SOUTH
Post Office Box 55305
BIRMINGHAM, ALABAMA 35255-5305
Principal Investigator: D. H. Pontius
Task Leader: T. R. Snyder

for

UNITED STATES DEPARTMENT OF ENERGY
Federal Energy Technology Center - Morgantown
Post Office Box 880, 3610 Collins Ferry Road
Morgantown, West Virginia 26505

Contract No. DE-AC21-94MC31160
Project Manager: Thomas P. Dorchak

Abstract

This is the final technical report describing the activities performed under Task 1 of Contract No. DE-AC21-94MC31160. The analyses of hot gas stream cleanup (HGCU) particulate samples and descriptions of filter performance studied under this contract were designed to address problems with filter operation that have been linked to characteristics of the collected particulate matter. One objective of this work was to generate an interactive, computerized data bank of the key physical and chemical characteristics of ash and char collected from operating advanced particle filters and to relate these characteristics to the operation and performance of these filters. The interactive data bank summarizes analyses of over 160 ash and char samples from fifteen pressurized fluidized-bed combustion and gasification facilities utilizing high-temperature, high pressure barrier filters. As a deliverable item under this contract, the HGCU data bank was to be submitted to the Department of Energy by the closing date of the contract (September 30, 1999). All of the data measured and activities conducted under Task 1 of Contract DE-AC21-94MC31160, and a significant proportion of data and activities generated under a prior contract with DOE/FETC (Contract No. DE-AC21-89MC26239) are presented in this final report.

TABLE OF CONTENTS

	<u>PAGE</u>
1.0 EXECUTIVE SUMMARY	1-1
2.0 INTRODUCTION.....	2-1
2.1 OBJECTIVES	2-1
3.0 FIELD SAMPLING AND ON-SITE MEASUREMENTS.....	3-1
3.1 TIDD	3-2
3.1.1 September 30, 1993.....	3-3
3.1.2 May 5, 1994.....	3-7
3.1.3 October 27, 1994.....	3-16
3.1.4 May 11, 1995.....	3-24
3.2 DOE/FETC MODULAR GAS CLEANUP RIG	3-31
3.2.1 October 29, 1996	3-31
3.3 POWER SYSTEMS DEVELOPMENT FACILITY	3-33
3.3.1 April 9, 1997	3-34
3.3.2 July 29, 1997	3-39
3.3.3 November 5, 1997.....	3-40
3.3.4 January 20, 1998.....	3-44
3.3.5 May 18, 1998.....	3-51
3.3.6 January 26, 1999.....	3-56
4.0 ANALYSES OF PARTICULATE SAMPLES.....	4-1
4.1 LABORATORY METHODS USED TO CHARACTERIZE SAMPLES	4-1
4.2 TIDD	4-7
4.3 KARHULA PRESSURIZED CIRCULATING FLUID BED FACILITY	4-40
4.4 DOE/FETC MODULAR GAS CLEANUP RIG	4-50
4.5 POWER SYSTEMS DEVELOPMENT FACILITY	4-60
4.6 PIÑON PINE POWER PROJECT	4-74
4.7 TRANSPORT REACTOR DEVELOPMENT UNIT	4-95
4.8 HERMAN RESEARCH PTY LTD.	4-114
4.9 ADDITIONAL ANALYSES	4-123
4.9.1 Characterization of Additional Gasifier Char Samples.....	4-123
4.9.2 Laboratory Baking of Ash Nodules.....	4-146
4.9.3 Additive Conditioning Tests	4-147
4.9.4 Ash Compaction Tests	4-149
5.0 MODELING PARTICULATE BEHAVIOR	5-1
5.1 EMPIRICAL PERMEABILITY MODEL	5-1
5.2 EFFECT OF NON-UNIFORM DUST CAKE POROSITY ON GAS FLOW	5-2
5.3 TRANSLATING LABORATORY PERMEABILITY DATA TO HGCU CONDITIONS.....	5-6
5.4 PERMEABILITY AS A FUNCTION OF GAS PRESSURE.....	5-7
5.5 REPRODUCIBILITY OF MEASUREMENTS.....	5-9
5.5.1 Specific Gas-Flow Resistance.....	5-9
5.5.2 Uncompacted Bulk Porosity.....	5-9
5.6 EFFECT OF SCREEN MESH SIZE ON UNCOMPACTED BULK POROSITY	5-10

5.7 ESTIMATING FILTER VESSEL INERTIAL COLLECTION FROM SIZE DISTRIBUTION DATA	5-11
5.8 CONSOLIDATION AND BRIDGING OF PFBC ASH DEPOSITS IN HGCU FILTERS.....	5-15
5.9 PERFORMANCE ESTIMATES FOR DOE/FETC MGCR PARTICULATE RESIDUE.....	5-30
6.0 INTERACTIVE DATA BANK	6-1
7.0 CONCLUSIONS	7-1
7.1 OPPORTUNITIES FOR FUTURE WORK.....	7-3
8.0 REFERENCES.....	8-1
APPENDIX A TECHNIQUE FOR PRESERVING FILTER CAKES.....	A-1
APPENDIX B SAMPLE INFORMATION FORMS	B-1

LIST OF TABLES

TABLE #	TITLE	PAGE
Table 2-1	Overview of Facilities and Particulate Samples.....	2-2
Table 3-1	Filter Cake Areal Density Measurements (November 5, 1997)	3-43
Table 3-2	Filter Cake Thickness Measurements (November 5, 1997).....	3-44
Table 3-3	Filter Cake Thickness and Areal Density Measurements (January 20, 1998).....	3-46
Table 3-4	Filter Cake Areal Density and Thickness Measurements.....	3-55
Table 3-5	Filter Cake Areal Density and Thickness Measurements.....	3-62
Table 4-1	Tidd Ash and Sorbent Samples Analyzed in the Laboratory	4-8
Table 4-2	Abbreviations for Locations from which Ash Samples were Obtained	4-9
Table 4-3	Chemical Analyses of Selected Tidd Ashes and Sorbents, % wt.....	4-9
Table 4-4	Chemical Analyses of Additional Tidd Ashes, % wt.....	4-10
Table 4-5	Physical Characteristics of Selected Tidd Ash Samples	4-10
Table 4-6	Physical Characteristics of Selected Tidd Ash Samples	4-11
Table 4-7	Physical Characteristics of Selected Tidd Ash Samples	4-11
Table 4-8	Physical Characteristics of Selected Tidd Ash Samples	4-11
Table 4-9	Sieve Analyses of Tidd Ashes.....	4-12
Table 4-10	Chemical Analyses of Selected Tidd Ashes Collected in May, 1995, % wt.....	4-14
Table 4-11	Porosity of Tidd Ash Nodules	4-16
Table 4-12	Identification of Karhula Ash Samples Analyzed under this Task	4-40
Table 4-13	Physical Characteristics of Karhula Ash Samples.....	4-41
Table 4-14	Chemical Composition of Karhula Ashes, % wt.....	4-41
Table 4-15	Identification of DOE/FETC-MGN MGCR Gasification Particulate Samples.....	4-50
Table 4-16	Physical Characteristics of DOE/FETC MGCR Gasification Particulate Samples.....	4-50
Table 4-17	Chemical Characteristics of DOE/FETC MGCR Gasification Particulate Samples, % wt.	4-51
Table 4-18	Identification of PSDF Ash Samples Analyzed and Discussed in this Section	4-60
Table 4-19	Physical Characteristics of PSDF Ash Samples.....	4-61
Table 4-20	Average Filter Cake Porosity Values Measured during PSDF Site Visits	4-61
Table 4-21	Chemical Composition of PSDF Ashes, % wt.....	4-62
Table 4-22	Identification of Piñon Pine Samples Received for Analysis.....	4-75
Table 4-23	Physical Analyses of Piñon Pine Char Samples.....	4-75
Table 4-24	Measured Chemical Characteristics of Piñon Pine Char Samples, % wt.	4-76

Table 4-25	Size Distribution Data Measured for Piñon Pine Filter Fines (ID # 4316) with a Bahco Aerodynamic Classifier.....	4-77
Table 4-26	Selected Chemical Constituents Measured for Piñon Pine Filter Fines (ID # 4316) and Six Selected Size Fractions	4-77
Table 4-27	C-H-N Analyses of Six Selected Size Fractions of Piñon Pine Filter Fines (ID # 4316).....	4-77
Table 4-28	Identification of TRDU Samples.....	4-96
Table 4-29	Additional Identification of TRDU Samples.....	4-96
Table 4-30	Physical Characteristics of TRDU Samples.....	4-97
Table 4-31	Chemical Composition of TRDU Samples, % wt.....	4-97
Table 4-32	Identification of HRL Gasification Chars Received for Analysis	4-114
Table 4-33	Physical Characteristics of Herman Research Pty Ltd. Gasification Particulate Samples.....	4-115
Table 4-34	Chemical Characteristics of Herman Research Pty Ltd. Gasification Particulate Samples, % wt.	4-115
Table 4-35	Additional Gasifier Char Samples from the HGCU Data Bank.....	4-123
Table 4-36	Physical Characteristics of Texaco and Kellogg Brown & Root Gasification Chars	4-124
Table 4-37	Physical Characteristics of KRW Gasification Chars	4-124
Table 4-38	Chemical Analyses of Kellogg Brown & Root Gasification Chars, % wt.....	4-125
Table 4-39	Effects of Baking Duration at 1550 °F on the Porosity of a Tidd Nodule (ID # 4097; BP, TS).....	4-146
Table 4-40	Characteristics of Additives Used to Condition HGCU Hopper Ashes.....	4-148
Table 4-41	Uncompacted Bulk Porosities of Mixtures of Hopper Samples and Conditioning Additives	4-148
Table 5-1	Assumed Distributions of Volume, Mass, and Porosity for Series and Parallel Examples (Configurations II and III in Figure 5-1).....	5-5
Table 5-2	Comparison of Laboratory Conditions with Typical HGCU Filter Conditions	5-6
Table 5-3	Specific Gas-Flow Resistance Measurements of PSDF Filter Cake Ash (ID # 4294)	5-9
Table 5-4	Uncompacted Bulk Porosity Measurements of PSDF Filter Cake Ash (ID # 4294)	5-10
Table 5-5	Uncompacted Bulk Porosity Measurements of PSDF Filter Cake Ash (ID # 4294)	5-10
Table 5-6	Selected Systems Containing Compounds that can Combine and Melt Below 1600 °F	5-23
Table 6-1	Analytical Quantities that can be Selected and Plotted as part of Interactive Querying	6-4
Table 6-2	HGCU Facilities Represented in the Data Bank	6-6

LIST OF FIGUES

FIGURE #	TITLE	PAGE
Figure 1-1	Ranges measured for some of the key physical characteristics of the filter cake samples discussed in this report.	1-3
Figure 3-1	General features of the APF at the Tidd Demonstration Plant.	3-3
Figure 3-2	Severe ash bridging was evident as the top two plenums were lifted into view.	3-4
Figure 3-3	Thick, patchy cakes were present throughout the filter vessel.	3-5
Figure 3-4	Ash almost completely enveloped many of the candle filter elements.	3-5
Figure 3-5	The appearance of these candles is believed to be the result of patchy cleaning and the loss of cake during cooling down of the filter vessel.	3-6
Figure 3-6	A number of laboratory analyses were performed on this thick filter cake deposit (ID # 4012). The deposition layers formed during filtration are clearly visible in this specimen.	3-6
Figure 3-7	Severe bridging and candle deformation in the top plenum.	3-8
Figure 3-8	A view of the top and middle plenums as the assembly was lifted from the filter vessel.	3-8
Figure 3-9	Portions of the top and middle plenums are visible in this photograph.	3-9
Figure 3-10	The entire plenum assembly being transported to the inspection platform.	3-9
Figure 3-11	Plenums being lowered into the inspection platform.	3-10
Figure 3-12	The interior of the filter vessel and the shroud after removal of the plenum assembly.	3-10
Figure 3-13	Close up of ash bridges and tubesheet deposits.	3-11
Figure 3-14	Bridging was especially severe adjacent to the central support column.	3-11
Figure 3-15	Bridging adjacent to the central support columns was pervasive.	3-12
Figure 3-16	In addition to deposits adjacent to the support columns, large, strong agglomerates formed around the regions where the candles were attached to the tubesheet.	3-12
Figure 3-17	Close up of ash bridges.	3-13
Figure 3-18	Two types of fracture surfaces are seen here. The relatively clean fracture surfaces on the two elements in the foreground indicate that these elements broke following operation. The ash-covered fracture surface of the element just to the right of the aforementioned elements indicates that this element broke before operation was discontinued.	3-13
Figure 3-19	Large ash deposits were common under the tubesheet. This photograph also shows the general appearance of the filter cakes.	3-14

Figure 3-20	The candles in the bottom plenums were relatively free of bridges, presumably because these plenums had no support columns in the center of the arrays of elements. (Deposits formed by turbulent diffusion on the central columns in the upper plenums. These deposits grew unabated, and significantly contributed to the problems that were common in the upper plenums.) 3-14	3-14
Figure 3-21	The bottom plenum was not entirely free of bridging between candles. This photograph shows a chunk of ash stuck between candles in the bottom plenum. This chunk is believed to have originated under the tubesheet in the bottom plenum. 3-15	3-15
Figure 3-22	Close up of the filter cakes in the bottom plenum..... 3-15	3-15
Figure 3-23	At various places large ash deposits were found lodged between filter elements..... 3-16	3-16
Figure 3-24	General appearance of the top plenum as it was being transported to the inspection platform..... 3-17	3-17
Figure 3-25	The top plenum experienced some bridging and broken elements. 3-18	3-18
Figure 3-26	This photograph shows a cover that was installed to minimize the growth of ash deposits around the tubesheet..... 3-18	3-18
Figure 3-27	This photograph shows the general condition of the bottom and middle plenums as they were lifted from the filter vessel..... 3-19	3-19
Figure 3-28	Some ash bridges were observed at the bottom of the middle plenum. 3-19	3-19
Figure 3-29	General condition of top and middle plenums as they were transported to the inspection platform..... 3-20	3-20
Figure 3-30	General condition of middle and bottom plenums as they were transported to the inspection platform..... 3-20	3-20
Figure 3-31	View of a tubesheet ash deposit on the bottom plenum..... 3-21	3-21
Figure 3-32	View of a tubesheet ash deposit on the top plenum. 3-21	3-21
Figure 3-33	Condition of the tubesheet and top portion of the top plenum..... 3-22	3-22
Figure 3-34	This morphology of this large ash bridge supports the conclusion that loose ash falling from above can be blocked and retained by chunks of ash previously lodged against the candles. This bridge was located near the lower end of the filter elements just above the conical surface of the ash shed..... 3-22	3-22
Figure 3-35	Chunks of ash that get trapped between candles (as shown here) appear to provide the initial conditions for development of bridges between adjacent filter elements. Ash removed during cleaning pulses piles on top of these trapped chunks instead of falling into the hopper for removal..... 3-23	3-23
Figure 3-36	This view looking up at the middle plenum shows six candles that broke during operation. The appearance of the central support column suggests that cleaning pulses passing downward through these six locations scoured the column clean..... 3-23	3-23

Figure 3-37	The filter assembly was basically free of bridges and most of the elements were intact when the assembly was removed from the filtration vessel.	3-24
Figure 3-38	Breakages in the plenum on the left were attributed to factors other than ash characteristics.....	3-25
Figure 3-39	The middle plenum assembly was clean and the filter elements were intact.	3-25
Figure 3-40	The bottom plenum was clean and the filter elements were intact. The filter assembly is being lowered onto the inspection platform.....	3-26
Figure 3-41	The intact candles in the top plenum were very clean.....	3-26
Figure 3-42	Only minor deposits were present on the ash shed below the top plenum.	3-27
Figure 3-43	The distinctly different appearances of the filter cakes on these two filter arrays in the bottom plenum are believed to be a result of different element types.	3-27
Figure 3-44	Close up of filter cakes in the bottom plenum.	3-28
Figure 3-45	Many of the filter cakes were moderately thick and irregular in shape.....	3-28
Figure 3-46	Tubesheet region of the bottom plenum.....	3-29
Figure 3-47	This view looking up at the top two plenums shows how the inner ring of elements was removed prior to this run, and how the elements remained relatively clean.....	3-29
Figure 3-48	The ash sheds remained relatively clean during this run.....	3-30
Figure 3-49	The intact elements in the top plenum remained clean.	3-30
Figure 3-50	The ash sheds and the central support columns remained free of significant ash deposits.	3-31
Figure 3-51	Lower portion of the four candles removed from the MGCR filter vessel. Each element was covered with a thin, black filter cake that was smooth and fluffy.	3-32
Figure 3-52	Microscopic examination of the filter cakes was used to determine their thickness.....	3-32
Figure 3-53	Removal of the filter assembly for inspection and refitting.....	3-35
Figure 3-54	Typical condition of the filter cakes.....	3-35
Figure 3-55	Lower plenum candles.....	3-36
Figure 3-56	The lower plenum clearing the filtration vessel.	3-36
Figure 3-57	Typical deposits that formed around the filter element mounting assemblies.....	3-37
Figure 3-58	Typical patchy cakes observed on the filter elements.	3-37
Figure 3-59	Upper portion of the top plenum assembly.	3-38
Figure 3-60	Lower portion of the top plenum assembly.....	3-38
Figure 3-61	Upper portion of candles showing impaction ridges in the filter cakes.	3-39
Figure 3-62	Interior of the filter vessel showing the shroud that surrounds the plenums.....	3-40

Figure 3-63	Filter cakes and deposits at the top of the filter elements. The blue color in this photograph was caused by blue tarps surrounding the inspection platform.	3-41
Figure 3-64	Lower portion of some of the candles on the lower plenum. The blue color in this photograph was caused by blue tarps surrounding the inspection platform.	3-41
Figure 3-65	More deposits around the top of the filter elements. The blue color in this photograph was caused by blue tarps surrounding the inspection platform.	3-42
Figure 3-66	Upper half of the lower plenum assembly. The blue color in this photograph was caused by blue tarps surrounding the inspection platform.....	3-42
Figure 3-67	Upper portion of filter elements. The blue color in this photograph was caused by blue tarps surrounding the inspection platform.....	3-43
Figure 3-68	Pressure drop data from FL0301 operation early on December 8, 1997.....	3-45
Figure 3-69	Many of the filter cakes observed on January 20, 1998 had a lumpy appearance.	3-47
Figure 3-70	Deposits observed around the top of the filter elements.	3-48
Figure 3-71	Typical appearance of the lower portion of the filter elements.....	3-48
Figure 3-72	A representative photograph of the appearance of the majority of the filter cakes observed in the Siemens Westinghouse FL0301 filter at the PSDF on January 20, 1998.	3-49
Figure 3-73	A representative photograph of the appearance of one of the lumpier filter cakes observed in the Siemens Westinghouse FL0301 filter at the PSDF on January 20, 1998.	3-49
Figure 3-74	A representative photograph of the appearance of a relatively smooth filter cake observed in the Siemens Westinghouse FL0301 filter at the PSDF on January 20, 1998.	3-50
Figure 3-75	A representative photograph of the appearance of the smoothest filter cakes observed in the Siemens Westinghouse FL0301 filter at the PSDF on January 20, 1998. Small pinholes are distributed over the surface of the cake.	3-50
Figure 3-76	A representative photograph of the appearance of a passive ash deposit formed on a set of stacked samples of various filter element materials located within the array of candle filter elements. This deposit was observed in the Siemens Westinghouse FL0301 filter at the PSDF on January 20, 1998.	3-51
Figure 3-77	Appearance of the entire filter assembly on May 18, 1998 during removal from the filter vessel.	3-52
Figure 3-78	Close up of plenum assembly during transport to the inspection platform.....	3-53
Figure 3-79	Typical smooth filter cakes observed on the bottom filter plenum at the PSDF on May 18, 1998.	3-53

Figure 3-80	Close up of relatively smooth filter cake.....	3-54
Figure 3-81	Another close up of relatively smooth filter cake.	3-54
Figure 3-82	This photograph shows the typical ash deposits formed around the mounting locations on the top filter plenum at the PSDF (May 18, 1998).....	3-55
Figure 3-83	FL0301 filter assembly being transported to the inspection platform on January 26, 1999.....	3-56
Figure 3-84	FL0301 filter assembly being transported to the inspection platform on January 26, 1999.....	3-57
Figure 3-85	Overall view of candles in the top plenum (January 26, 1999).....	3-57
Figure 3-86	Close up of filter cake in the top plenum (January 26, 1999).	3-58
Figure 3-87	Typical deposits that formed around the filter element mounting assemblies (January 26, 1999).....	3-58
Figure 3-88	Lower portion of filter elements in the top plenum (January 26, 1999).....	3-59
Figure 3-89	Close up of a filter cake in the top plenum (January 26, 1999).....	3-59
Figure 3-90	Lower portion of the filter elements in the top plenum (January 26, 1999).	3-60
Figure 3-91	Many of the filter cakes observed in the top plenum on January 26, 1999 had a lumpy appearance.	3-60
Figure 3-92	Another view of lumpy filter cakes observed in the top plenum on January 26, 1999.....	3-61
Figure 4-1	Typical curves showing the dependence of gas-flow resistance on porosity. The only difference between the curves is a scale factor ($1/D^2$), where D = the drag-equivalent diameter.	4-3
Figure 4-2	Schematic diagram of the electrostatic tensiometer.	4-6
Figure 4-3	Cumulative size distribution data measured with a sedigraph and sieves for five ashes collected from the Tidd APF. The hollow data points represent sedigraphically obtained diameters. The filled data points represent data obtained in the sieve analyses.	4-13
Figure 4-4	Representative SEM photographs of Tidd filter cake ash (ID # 4144) taken at a) 100X, b) 500X, c) 1000X, and d) 5000X.	4-17
Figure 4-5	Representative SEM photographs of size fractionated Tidd filter cake ash (ID # 4320, diameter > 45 μm) taken at a) 100X, b) 500X, c) 1000X, and d) 5000X.....	4-18
Figure 4-6	Representative SEM photographs of size fractionated Tidd filter cake ash (ID # 4321, 15 μm < diameter < 45 μm) taken at a) 100X, b) 500X, c) 1000X, and d) 5000X.....	4-19
Figure 4-7	Representative SEM photographs of size fractionated Tidd ash taken from a tube sheet deposit (ID # 4151) taken at a) 100X, b) 500X, c) 1000X, and d) 5000X.....	4-20

Figure 4-8	Representative SEM photographs of size fractionated Tidd ash taken from a tube sheet deposit (ID # 4322, diameter > 45 μm) taken at a) 100X, b) 500X, c) 1000X, and d) 5000X.....	4-21
Figure 4-9	Representative SEM photographs of size fractionated Tidd ash taken from a tube sheet deposit (ID # 4323, 15 μm < diameter < 45 μm) taken at a) 100X, b) 500X, c) 1000X, and d) 5000X.....	4-22
Figure 4-10	Representative SEM photographs of Tidd ash from the hopper of the cyclone upstream of the APF (ID # 2791) taken at a) 100X, b) 500X, c) 1000X, and d) 5000X.....	4-23
Figure 4-11	Representative SEM photographs of Tidd APF hopper ash (ID # 2822) taken at a) 100X, b) 500X, c) 1000X, and d) 5000X.	4-24
Figure 4-12	Representative SEM photographs of Tidd APF hopper ash (ID # 2823) taken at a) 100X, b) 500X, c) 1000X, and d) 5000X.	4-25
Figure 4-13	Representative SEM photographs of Tidd APF hopper ash (ID # 2824) taken at a) 100X, b) 500X, c) 1000X, and d) 5000X.	4-26
Figure 4-14	Representative SEM photographs of Tidd ash (ID # 4114; MP,AS) taken at a) 100X, b) 500X, c) 1000X, and d) 5000X.....	4-27
Figure 4-15	Scanning electron micrograph of a fresh internal fracture surface of a filter cake ash nodule from Tidd (ID # 4012). The white bars at the bottom of the micrograph represent lengths of 10 μm. Locations where EDX spectra were measured are identified on this figure.	4-29
Figure 4-16	Scanning electron micrograph of a fresh internal fracture surface of a filter cake ash nodule from Tidd (ID # 4012). The white bar at the bottom of the micrographs represents a length of 10 μm. Locations where EDX spectra were measured are identified on this figure.	4-29
Figure 4-17	EDX spectrum taken at location P1 on the fracture surface of the Tidd filter cake nodule shown in Figure 4-15.....	4-30
Figure 4-18	EDX spectrum taken at location P2 on the fracture surface of the Tidd filter cake nodule shown in Figure 4-15.....	4-30
Figure 4-19	EDX spectrum taken at location B1 on the fracture surface of the Tidd filter cake nodule shown in Figure 4-15.....	4-31
Figure 4-20	EDX spectrum taken at location P3 on the fracture surface of the Tidd filter cake nodule shown in Figure 4-15.....	4-31
Figure 4-21	EDX spectrum taken at location P4 on the fracture surface of the Tidd filter cake nodule shown in Figure 4-15.....	4-32
Figure 4-22	EDX spectrum taken at location P5 on the fracture surface of the Tidd filter cake nodule shown in Figure 4-15.....	4-32
Figure 4-23	EDX spectrum taken at location B2 on the fracture surface of the Tidd filter cake nodule shown in Figure 4-15.....	4-33
Figure 4-24	EDX spectrum taken at location P6 on the fracture surface of the Tidd filter cake nodule shown in Figure 4-15.....	4-33
Figure 4-25	EDX spectrum taken at location P7 on the fracture surface of the Tidd filter cake nodule shown in Figure 4-15.....	4-34

Figure 4-26	EDX spectrum taken at location B3 on the fracture surface of the Tidd filter cake nodule shown in Figure 4-15.....	4-34
Figure 4-27	EDX spectrum taken at location P8 on the fracture surface of the Tidd filter cake nodule shown in Figure 4-15.....	4-35
Figure 4-28	EDX spectrum taken at location P9 on the fracture surface of the Tidd filter cake nodule shown in Figure 4-15.....	4-35
Figure 4-29	EDX spectrum taken at location B4 on the fracture surface of the Tidd filter cake nodule shown in Figure 4-15.....	4-36
Figure 4-30	EDX spectrum taken at location P1 on the fracture surface of the Tidd filter cake nodule shown in Figure 4-16.....	4-36
Figure 4-31	EDX spectrum taken at location P2 on the fracture surface of the Tidd filter cake nodule shown in Figure 4-16.....	4-37
Figure 4-32	EDX spectrum taken at location B1 on the fracture surface of the Tidd filter cake nodule shown in Figure 4-16.....	4-37
Figure 4-33	EDX spectrum taken at location P3 on the fracture surface of the Tidd filter cake nodule shown in Figure 4-16.....	4-38
Figure 4-34	EDX spectrum taken at location B2 on the fracture surface of the Tidd filter cake nodule shown in Figure 4-16.....	4-38
Figure 4-35	Micrographs of a fresh fracture surface of an ash agglomerate (ID # 4114) taken from an ash shed in the Tidd APF in October 1994.	4-39
Figure 4-36	Cumulative and differential size distribution of Karhula filter cake ash (ID # 4182) measured with a sedigraph.....	4-42
Figure 4-37.	Cumulative size distributions of Karhula filter cake ash (ID # 4277) and hoppper ash (ID # 4276) measured with a Bahco aerodynamic classifier. ..	4-43
Figure 4-38	Cumulative and differential size distribution data measured for Karhula hopper ash (ID # 4276) and filter cake ash (ID # 4277) measured with a Leeds and Northrup Microtrac Particle Size Analyzer. The size distribution of the filter cake ash has been linearly scaled down by a factor of 0.36 to cause the shape of the finer portions of these two distributions to coincide as much as possible.....	4-44
Figure 4-39	Cumulative and differential size distribution data measured for Karhula hopper ash (ID # 4276) measured with a Leeds and Northrup Microtrac Analyzer. The difference of the size distribution of the filter cake ash (ID # 4277) presented in Figure 4-38 has been subtracted from the size distribution of the hopper ash to display the size distribution of the particles assumed to have settled out in the hopper without having ever reached the filter cake surface.	4-45
Figure 4-40	Micrographs of filter cake ash from the Karhula PCFB (ID # 4182) taken at a) 100X, b) 500X, and c) 5000X.....	4-46
Figure 4-41	Micrographs of filter cake ash from the Karhula PCFB (ID # 4277) taken at a) 100X, b) 500X, c) 1000X, and d) 10,000X.....	4-47
Figure 4-42	Representative micrographs of DOE/FETC MGCR gasifier char (ID # 4170) taken at a) 500X, b) 1000X, c) 5000X, and d) 10,000X.....	4-52

Figure 4-43	Representative micrographs of DOE/FETC MGCR gasification char (ID # 4198) taken at a) 500X, a) 1000X, c) 5000X and d) 10,000X.	4-53
Figure 4-44	Cumulative and differential size distribution data measured for ash from the DOE/FETC gasifier (ID # 4170) measured with a Shimadzu SA-CP4 Centrifugal Particle Size Analyzer. The MMD of this distribution is 0.74 μm , and its geometric standard deviation is 2.8 μm . (This size distribution data includes the assumption that the ash contains no particles smaller than 0.063 μm .)	4-54
Figure 4-45	Cumulative and differential size distribution data measured for DOE/FETC-MGN MGCR gasification particulate (ID # 4198) measured with a Shimadzu SA-CP4 Centrifugal Particle Size Analyzer. The MMD of this distribution, which appears to be bimodal, is 0.76 μm , and its geometric standard deviation is 3.1. (This size distribution data includes the assumption that the sample contains no particles smaller than 0.063 μm .)	4-55
Figure 4-46	Cumulative and differential size distribution data measured for DOE/FETC-MGN MGCR gasification particulate (ID # 4259) measured with a Shimadzu SA-CP4 Centrifugal Particle Size Analyzer. The MMD of this distribution, which appears to be bimodal, is 0.29 μm , and its geometric standard deviation is 2.3. (This size distribution data includes the assumption that the sample contains no particles smaller than 0.063 μm .)	4-56
Figure 4-47	Data calculated with the permeability model for the DOE/FETC MGCR gasification char (ID # 4170) showing the strong dependence of specific gas-flow resistance on filter cake porosity.	4-58
Figure 4-48	Response of sample ID # 4170 to mechanically applied compacting forces.....	4-59
Figure 4-49	Cumulative and differential size distribution data measured for PSDF filter cake ash (ID # 4239) measured with a Shimadzu SA-CP4 Centrifugal Particle Size Analyzer. The MMD of this distribution is 6.9 μm , and its geometric standard deviation is 2.8. The D_{16} of this distribution is 1.9 μm , and its D_{84} is 15 μm . (This size distribution data includes the assumption that the sample contains no particles smaller than 0.063 μm .)	4-63
Figure 4-50	Cumulative and differential size distribution data measured for PSDF filter cake ash (ID # 4245) measured with a Shimadzu SA-CP4 Centrifugal Particle Size Analyzer. The MMD of this distribution is 7.9 μm , and its geometric standard deviation is 2.9. The D_{16} of this distribution is 2.4 μm , and its D_{84} is 20 μm . (This size distribution data includes the assumption that the sample contains no particles smaller than 0.063 μm .)	4-64

Figure 4-51	Cumulative and differential size distribution data measured for PSDF filter cake ash (ID # 4231) measured with a Shimadzu SA-CP4 Centrifugal Particle Size Analyzer. The MMD of this distribution is 4.7 μm , and its geometric standard deviation is 3.3. The D_{16} of this distribution is 1.4 μm , and its D_{84} is 15 μm . (This size distribution data includes the assumption that the sample contains no particles smaller than 0.063 μm .)4-65
Figure 4-52	Cumulative and differential size distribution data measured for PSDF filter cake ash (ID # 4232) measured with a Shimadzu SA-CP4 Centrifugal Particle Size Analyzer. The MMD of this distribution is 9.9 μm , and its geometric standard deviation is 3.2. The D_{16} of this distribution is 2.3 μm , and its D_{84} is 23 μm . (This size distribution data includes the assumption that the sample contains no particles smaller than 0.063 μm .)4-66
Figure 4-53	Cumulative and differential size distribution data measured for PSDF filter cake ash (ID # 4233) measured with a Shimadzu SA-CP4 Centrifugal Particle Size Analyzer. The MMD of this distribution is 8.1 μm , and its geometric standard deviation is 2.9. The D_{16} of this distribution is 2.3 μm , and its D_{84} is 19 μm . (This size distribution data includes the assumption that the sample contains no particles smaller than 0.063 μm .)4-67
Figure 4-54	Cumulative and differential size distribution data measured for PSDF filter cake ash (ID # 4258) measured with a Shimadzu SA-CP4 Centrifugal Particle Size Analyzer. The MMD of this distribution is 4.6 μm , and its geometric standard deviation is 2.6. The D_{16} of this distribution is 1.6 μm , and its D_{84} is 11 μm . (This size distribution data includes the assumption that the sample contains no particles smaller than 0.063 μm .)4-68
Figure 4-55	Cumulative and differential size distribution data measured for PSDF filter cake ash (ID # 4262) measured with a Shimadzu SA-CP4 Centrifugal Particle Size Analyzer. The D_{16} of this distribution is 1.2 μm , its D_{50} is 3.8 μm , its D_{84} is 13 μm , and its geometric standard deviation is 3.8. (These size distribution data include the assumption that the sample contains no particles smaller than 0.063 μm .).....4-69
Figure 4-56	Representative scanning electron micrographs of PSDF filter cake ash (ID # 4233) taken at a) 100X, b) 1000X, and c) 5000X.4-71
Figure 4-57	Representative scanning electron micrographs of PSDF filter cake ash (ID # 4257) taken at a) 100X, b) 1000X, and c) 5000X.4-72
Figure 4-58	Representative scanning electron micrographs of PSDF filter cake ash (ID # 4262) taken at a) 100X, b) 500X, c) 1000X, and d) 5000X.4-73
Figure 4-59	Scanning electron micrograph of Piñon Pine IGCC Power Project filter fines particulate sample (ID # 4316). The white bar at the bottom of the micrograph represents a length of 100 μm4-78
Figure 4-60	Scanning electron micrograph of Piñon Pine IGCC Power Project filter fines particulate sample (ID # 4316). The white bars at the bottom of the micrograph represent lengths of 10 μm4-78

Figure 4-61	Differential and cumulative size distribution data measured for Piñon Pine filter fines (ID # 4316) with a Leeds and Northrup Microtrac Particle Size Analyzer. The MMD of this distribution is 19 μm	4-79
Figure 4-62	Cumulative particle size of the Piñon Pine filter fines (ID # 4316) measured with a Bahco Aerodynamic Classifier.....	4-80
Figure 4-63	Carbon contents of the various size fractions of Piñon Pine filter fines (ID # 4316). The carbon content (50.7 %) of the size fraction of particles larger than 26.7 μm is not represented on this plot.	4-80
Figure 4-64	Representative scanning electron micrograph of Piñon Pine gasifier char (ID # 4349) collected in January 1999 from the filter hopper. The black and white bars at the bottom of the micrograph represent lengths of 100 μm	4-82
Figure 4-65	Representative scanning electron micrograph of Piñon Pine gasifier char (ID # 4349) collected in January 1999 from the filter hopper. The white bar at the bottom of the micrograph represents a length of 100 μm	4-82
Figure 4-66	Representative scanning electron micrograph of Piñon Pine gasifier char (ID # 4349) collected in January 1999 from the filter hopper. The black and white bars at the bottom of the micrograph represent lengths of 10 μm	4-83
Figure 4-67	Representative scanning electron micrograph of Piñon Pine gasifier char (ID # 4349) collected in January 1999 from the filter hopper. The white bar at the bottom of the micrograph represents a length of 10 μm	4-83
Figure 4-68	Representative scanning electron micrograph of Piñon Pine gasifier char (ID # 4350) collected in January 1999 as part of the filter cake. The black and white bars at the bottom of the micrograph represent lengths of 100 μm	4-84
Figure 4-69	Representative scanning electron micrograph of Piñon Pine gasifier char (ID # 4350) collected in January 1999 as part of the filter cake. The white bar at the bottom of the micrograph represents a length of 100 μm	4-84
Figure 4-70	Representative scanning electron micrograph of Piñon Pine gasifier char (ID # 4350) collected in January 1999 as part of the filter cake. The black and white bars at the bottom of the micrograph represent lengths of 10 μm	4-85
Figure 4-71	Representative scanning electron micrograph of Piñon Pine gasifier char (ID # 4350) collected in January 1999 as part of the filter cake. The white bar at the bottom of the micrograph represents a length of 10 μm	4-85
Figure 4-72	Differential size distribution data measured for Piñon Pine particulate matter collected in January 1999. The size distribution of the material collected in the filter hopper (ID # 4349) is overlaid with the size distribution of particulate matter collected as part of the filter cake (ID# 4350). A scaling factor of 0.80 was applied to the filter cake particulate size distribution to cause the finest portion of these two distributions to coincide.	4-86

Figure 4-73	Differential size distribution data measured for Piñon Pine particulate matter collected in January 1999. The size distribution of the filter hopper char is overlaid with the size distribution of particulate matter assumed to have settled into the hopper without ever reaching the surface of the filter cake.....	4-87
Figure 4-74	Representative scanning electron micrograph of a fresh fracture surface of a Piñon Pine gasifier char filter cake nodule (ID # 4350) collected in January 1999. The black and white bars at the bottom of the micrograph represent lengths of 10 μm	4-90
Figure 4-75	Representative scanning electron micrograph of a fresh fracture surface of a Piñon Pine gasifier char filter cake nodule (ID # 4350) collected in January 1999. The black and white bars at the bottom of the micrograph represent lengths of 10 μm	4-90
Figure 4-76	Representative scanning electron micrograph of a fresh fracture surface of a Piñon Pine gasifier char filter cake nodule (ID # 4350) collected in January 1999. The black and white bars at the bottom of the micrograph represent lengths of 10 μm . The locations where EDX spectra (Figures 4-77 through 4-83) were measured are labeled P1 through P7.....	4-91
Figure 4-77	EDX spectrum taken at location P1 in the Piñon Pine filter cake nodule shown in Figure 4-76.....	4-92
Figure 4-78	EDX spectrum taken at location P2 in the Piñon Pine filter cake nodule shown in Figure 4-76.....	4-92
Figure 4-79	EDX spectrum taken at location P3 in the Piñon Pine filter cake nodule shown in Figure 4-76.....	4-93
Figure 4-80	EDX spectrum taken at location P4 in the Piñon Pine filter cake nodule shown in Figure 4-76.....	4-93
Figure 4-81	EDX spectrum taken at location P5 in the Piñon Pine filter cake nodule shown in Figure 4-76.....	4-94
Figure 4-82	EDX spectrum taken at location P6 in the Piñon Pine filter cake nodule shown in Figure 4-76.....	4-94
Figure 4-83	EDX spectrum taken at location P7 in the Piñon Pine filter cake nodule shown in Figure 4-76.....	4-95
Figure 4-84	Cumulative size distribution of hopper ash from the UNDEERC TRDU (ID # 4176) measured with a Bahco aerodynamic classifier.....	4-98
Figure 4-85	Cumulative and differential size distribution data measured for UNDEERC TRDU PO50 filter vessel ash (ID # 4199) measured with a Shimadzu SA-CP4 Centrifugal Particle Size Analyzer. The MMD of this distribution is 2.4 μm , and its geometric standard deviation is 2.6. The D_{16} of this distribution is 0.93 μm , and its D_{84} is 6.1 μm . (This size distribution data includes the assumption that the sample contains no particles smaller than 0.063 μm .).....	4-99

Figure 4-86	Cumulative and differential size distribution data for P056 filter hopper char (ID # 4326) measured with a Leeds and Northrup Microtrac Particle Size Analyzer.	4-100
Figure 4-87	Cumulative and differential size distribution data for P056 filter hopper char (ID # 4327) measured with a Leeds and Northrup Microtrac Particle Size Analyzer.	4-101
Figure 4-88	Cumulative and differential size distribution data for P057 filter hopper char (ID # 4328) measured with a Leeds and Northrup Microtrac Particle Size Analyzer.	4-102
Figure 4-89	Cumulative and differential size distribution data for P057 filter hopper char (ID # 4329) measured with a Leeds and Northrup Microtrac Particle Size Analyzer.	4-103
Figure 4-90	Cumulative and differential size distribution data for P058 filter hopper ash (ID # 4330) measured with a Leeds and Northrup Microtrac Particle Size Analyzer.	4-104
Figure 4-91	Micrographs of hopper ash from the UNDEERC TRDU (ID # 4176) taken at a) 100X, b) 500X, and c) 5000X.	4-105
Figure 4-92	Representative scanning electron micrographs of UNDEERC TRDU PO50 filter vessel char (ID # 4199) taken at a) 500X, b) 1000X, c) 5000X and d) 10,000X.	4-106
Figure 4-93	Representative Scanning Electron Micrographs of P051 filter hopper char (ID # 4324) taken at magnifications of a) 100x, b) 500x, c) 1000x, and d) 5000x.	4-107
Figure 4-94	Representative Scanning Electron Micrographs of P051 filter cake char (ID # 4325) taken at magnifications of a) 100x, b) 500x, c) 1000x, and d) 5000x.	4-108
Figure 4-95	Representative Scanning Electron Micrographs of P056 filter hopper char (ID # 4327) taken at magnifications of a) 100x, b) 500x, c) 1000x, and d) 5000x.	4-109
Figure 4-96	Representative Scanning Electron Micrographs of P057 filter hopper char (ID # 4329) taken at magnifications of a) 100x, b) 500x, c) 1000x, and d) 5000x.	4-110
Figure 4-97	Representative Scanning Electron Micrographs of P058 filter hopper ash (ID # 4330) taken at magnifications of a) 100x, b) 500x, c) 1000x, and d) 5000x.	4-111
Figure 4-98	Cumulative and differential size distribution data measured for Herman Research Pty Ltd. Mulgrave test rig (Morwell coal) gasification particulate (ID # 4195) measured with a Shimadzu SA-CP4 Centrifugal Particle Size Analyzer. The MMD of this distribution is 7.3 μm , and its geometric standard deviation is 3.4. (This size distribution data includes the assumption that the sample contains no particles smaller than 0.063 μm .)	4-116

Figure 4-99	Cumulative and differential size distribution data measured for Herman Research Pty Ltd. Mulgrave test rig (Loy Yang coal) gasification particulate (ID # 4196) measured with a Shimadzu SA-CP4 Centrifugal Particle Size Analyzer. The MMD of this distribution is 3.6 μm , and its geometric standard deviation is 7.0. (This size distribution data includes the assumption that the sample contains no particles smaller than 0.063 μm .)	4-117
Figure 4-100	Cumulative and differential size distribution data measured for Herman Research Pty Ltd. Mulgrave test rig (Yallourn coal) gasification particulate (ID # 4197) measured with a Shimadzu SA-CP4 Centrifugal Particle Size Analyzer. The MMD of this distribution is 7.2 μm , and its geometric standard deviation is 5.5. (This size distribution data includes the assumption that the sample contains no particles smaller than 0.063 μm .)	4-118
Figure 4-101	Representative scanning electron micrographs of Herman Research Pty Ltd. Mulgrave test rig (Morwell coal) gasification particulate (ID # 4195) taken at a) 100X, b) 500X, c) 1000X and d) 5000X.	4-119
Figure 4-102	Representative scanning electron micrographs of Herman Research Pty Ltd. Mulgrave test rig (Loy Yang coal) gasification particulate (ID # 4196) taken at a) 100X, b) 500X, c) 1000X and d) 5000X.	4-120
Figure 4-103	Representative scanning electron micrographs of Herman Research Pty Ltd. Mulgrave test rig (Yallourn coal) gasification particulate (ID # 4197) taken at a) 100X, b) 500X, c) 1000X and d) 5000X.	4-121
Figure 4-104	Representative scanning electron micrographs of Kellogg Brown & Root Transport Reactor Test Unit (TRTU) run G4 filter fines (ID # 2800) taken at a) 100X, b) 500X, c) 1000X, and d) 5000X.	4-126
Figure 4-105	Representative scanning electron micrographs of Kellogg Brown & Root TRTU run G101 filter fines (ID # 2803) taken at a) 100X, b) 500X, c) 1000X, and d) 5000X.	4-127
Figure 4-106	Representative scanning electron micrographs of Kellogg Brown & Root TRTU run H-1962-G3A filter fines (ID # 2832) taken at a) 100X, b) 500X, c) 1000X, and d) 5000X.	4-128
Figure 4-107	Representative scanning electron micrographs of Kellogg Brown & Root TRTU run H-1962-G5C filter fines (ID # 2834) taken at a) 100X, b) 500X, c) 1000X, and d) 5000X.	4-129
Figure 4-108	Representative scanning electron micrographs of Kellogg Brown & Root TRTU run H-1962-G7A filter fines (ID # 2838) taken at a) 100X, b) 500X, c) 1000X, and d) 5000X.	4-130
Figure 4-109	Representative scanning electron micrographs of Kellogg Brown & Root TRTU run H-1962-G8A filter fines (ID # 2840) taken at a) 100X, b) 500X, c) 1000X, and d) 5000X.	4-131

Figure 4-110	Representative scanning electron micrographs of Texaco Montebello Research Laboratory run L8902-04 filter vessel ash pot solids (ID # 2678) taken at a) 100X, b) 500X, c) 1000X, and d) 5000X.	4-132
Figure 4-111	Representative scanning electron micrographs of KRW fluidized bed gasification char (ID # 2550) taken at a) 100X, b) 500X, c) 1000X, and d) 5000X.	4-133
Figure 4-112	Representative scanning electron micrographs of KRW C-110 outlet composite gasification char (ID # 2556) taken at a) 100X, b) 500X, c) 1000X, and d) 5000X.	4-134
Figure 4-113	Representative scanning electron micrographs of KRW C-115 outlet composite gasification char (ID # 2557) taken at a) 100X, b) 500X, c) 1000X, and d) 5000X.	4-135
Figure 4-114	Representative scanning electron micrographs of KRW C-120 outlet composite gasification char (ID # 2558) taken at a) 100X, b) 500X, c) 1000X, and d) 5000X.	4-136
Figure 4-115	Representative scanning electron micrographs of KRW SC 41 hopper composite gasification char (ID # 2559) taken at a) 100X, b) 500X, c) 1000X, and d) 5000X.	4-137
Figure 4-116	Representative scanning electron micrographs of KRW C-121 hopper (4/25/88) gasification char (ID # 2560) taken at a) 100X, b) 500X, c) 1000X, and d) 5000X.	4-138
Figure 4-117	Representative scanning electron micrographs of KRW C-121 hopper (5/1/88) gasification char (ID # 2561) taken at a) 100X, b) 500X, c) 1000X, and d) 5000X.	4-139
Figure 4-118	Representative scanning electron micrographs of KRW C-121 hopper (4/28/88) gasification char (ID # 2562) taken at a) 100X, b) 500X, c) 1000X, and d) 5000X.	4-140
Figure 4-119	Representative scanning electron micrographs of KRW fluidized bed gasification char (ID # 2563) taken at a) 100X, b) 500X, c) 1000X, and d) 5000X. (This sample was collected via extractive sampling, and contained some fibers from the filter substrate.)	4-141
Figure 4-120	Drag-equivalent diameter as a function of specific surface area for char samples from a variety of HGCU installations.	4-143
Figure 4-121	Drag-equivalent diameter as a function of mass median diameter for char samples from a variety of HGCU installations.	4-145
Figure 4-122	Data measured for KRW gasification hopper char (ID # 2562) showing the dependence of porosity on mechanical pressure applied across the sample.	4-150

Figure 4-123	Data measured for the Tidd APF hopper ash (ID # 4049) showing the dependence of cake porosity on mechanical pressure applied across the cake. The procedures used to load the sample container caused initial differences in the porosity of the sample prior to compaction. As compacting pressure increased, the differences in porosity due to the different loading procedures diminish.....	4-151
Figure 5-1	Configurations for dust samples.....	5-2
Figure 5-2	Schematic diagram of a setup for evaluating the effect of absolute gas pressure on the specific gas-flow resistance of a particulate sample.	5-8
Figure 5-3	Cumulative and differential size distribution data for P051 filter cake char (ID # 4325) and filter hopper char (ID # 4324) measured with a Leeds and Northrup Microtrac Particle Size Analyzer. The differential data for the filter cake char in the lower graph have been scaled down by a factor of 0.673 to align the finest portion of its size distribution with that of the filter hopper char.	5-13
Figure 5-4	Cumulative and differential size distribution data for P051 filter hopper char (ID # 4324) and the portion of the char entering the filter vessel that is assumed to have settled out prior to reaching the surface of the candle filters. The calculation for assumed settling was derived from the comparison and scaling shown in Figure 5-3.....	5-14
Figure 5-5	Porosity gradient through one of the thick filter cake specimens collected on September 30, 1993 from the Tidd APF.	5-16
Figure 5-6	Scanning electron micrographs of internal fracture surfaces of a filter cake ash nodule from Tidd (ID # 4012). The white bars at the bottom of the micrographs represent lengths of 10 μm	5-17
Figure 5-7	Binary phase diagram showing the formation of a eutectic (AB) resulting from surface diffusion between solid compounds A and B in contact. Eutectic AB has a melting point less than the temperature of the HGCU filter. Compositions C_1 and C_2 have melting points equal to the temperature of the HGCU filter.....	5-20
Figure 5-8	Phase diagram for the system $\text{K}_2\text{SO}_4 - \text{MgSO}_4 - \text{CaSO}_4$	5-22
Figure 5-9	Schematic representation of the consolidation of ash deposits.	5-24
Figure 5-10	Mechanisms governing consolidation resulting from the formation of eutectic melts between PFBC ash particles.....	5-25
Figure 5-11	Sintering as a function of time for a range of particle sizes. Sintering is expressed as x/r , where x = the radius of the interparticle interface, and r = the particle radius.....	5-26
Figure 5-12	Sintering as a function of time for a range of viscosities. Sintering is expressed as x/r , where x = the radius of the interparticle interface, and r = the particle radius. Values of viscosity are given in poise.....	5-27
Figure 5-13	Diagram illustrating the various factors in a ceramic candle barrier filter collecting PFBC ash that can combine to cause filter failures.	5-29
Figure 6-1	Schematic representation of the portion of the data bank controlling the interactive querying and plotting of sample analyses data.	6-3

Figure 6-2 Schematic representation of the portion of the data bank controlling the review of project findings, site visits, background information on the HGCU facilities, and detailed analyses of individual samples.....6-5

Figure A-1 Schematic diagram of a device for using cyanoacrylate glue to strengthen filter cakes formed on a candle filter element in preparation for subsequent impregnation and encapsulation with low-viscosity epoxy.....A-3

1.0 EXECUTIVE SUMMARY

This is the final technical report describing the activities performed under Task 1 of Contract No. DE-AC21-94MC31160. The analyses of hot gas stream cleanup (HGCU) ashes and descriptions of filter performance studied under this contract were designed to address problems with filter operation that have been linked to characteristics of the collected ash. Task 1 was designed to generate an interactive, computerized data bank of the key characteristics of ash and char samples collected from pressurized fluidized-bed combustion (PFBC) and gasification facilities. This task was also designed to relate these characteristics to the operation and performance of operating advanced particle filters (APFs). APF operations have also been limited by the strength and durability of the ceramic materials that have served as barrier filters for the capture of entrained HGCU ashes. Task 2, which is summarized under a separate cover, concerned testing and failure analyses of ceramic filter elements currently used in operating APFs and the characterization and evaluation of new ceramic materials.

Ceramic barrier filters operating in HGCU environments face several potential challenges that may result from the characteristics of the ash or char being collected. The condition that has received the most attention since the first testing of these filters is the formation of tenacious ash deposits in the filter vessel that can form bridge-like structures that often result in lateral mechanical forces being exerted on the filter elements. Ash bridging can become extensive enough to significantly reduce active filter area, and ash deposits can become large enough to cause damage to filter elements if the deposits dislodge and fall to the hopper. Observations of the formation of high-strength ash deposits and ash bridging under this task were confined to PFBC facilities. Although experiences at American Electric Power Service Company's 70 MWe Tidd Pressurized Fluidized-Bed Combustor (Tidd) and Foster Wheeler's 10 MWt Pressurized Circulating Fluid Bed Facility in Karhula, Finland (Karhula) led to improved filter elements and filter system design to minimize the damaging effects of these ash deposits, operating experiences and supporting laboratory studies indicate that these improvements are not sufficient to completely remove the potential for ash bridges to form.¹ Residence time in the filter vessel, combined with filter temperature, and ash and flue gas chemistry, can provide conditions sufficient for strong PFBC ash deposits to form in HGCU filters. Although the fundamental mechanisms controlling the formation and strengthening of these ash deposits have not been completely verified, a great deal of information has been compiled characterizing PFBC ash deposits. Based on these characterizations, this task developed and presented a model of deposit growth based on the formation of eutectic compounds in PFBC ash.

Several approaches to limiting the potential for bridging have been tried. Bridging was significantly reduced at Tidd by limiting the time that ash remained in the APF.¹ At Karhula, various combinations of coals and sorbent materials were evaluated with one of the objectives being to minimize ash bridging.² At the Kellogg Brown & Root Advanced Transport Reactor at the Department of Energy / Southern Company Services Power Systems Development Facility (PSDF), the temperature of the filter vessel has not been allowed to approach the levels where severe bridging was encountered at Tidd. It is clear from the experiences at these facilities that understanding and optimizing ash characteristics is one of the keys to successful and optimized HGCU filter operation on PFBC systems.

In addition to bridging in HGCU filters, other key issues that are strongly dependent on the characteristics of the particles collected in the filter are pressure loss across the filter, the development of filter cakes that may be hard to remove during reverse-pulse cleaning, and the reentrainment and recollection on the filter cake of previously collected particles following their removal by cleaning pulses.

For a given filter design, the permeability of the filter cake is the primary variable determining overall pressure loss across the filter. (Although inlet mass concentration, filtering face velocity, gas viscosity, and the permeability of clean ceramic filter elements also contribute to the overall pressure loss, these factors are set by the system design.) Given these design factors, the pressure loss through the filter cake is determined by the amount of cake on the filter surface (usually expressed in terms of its areal density), and the morphology of the filter cake. This morphology is a combination of the porosity of the cake structure, and the morphology of the particles composing the cake. As with the other factors set by the system design, the morphology of the particles reaching the filter cake is determined by operating variables of the combustion or gasification system. Precollectors, such as cyclones upstream of the barrier filter can also modify particle morphology by preferentially removing the larger entrained particles.

Mathematical models of filtration, including the semi-empirical model refined under Task 1 of this contract describing the permeability of filter cakes composed of fine, irregular particles, demonstrate the sensitivity of flow resistance to cake porosity^{3,4,5,6,7}. Factors that can decrease the porosity of filter cakes in barrier filters include cake collapse caused by filtering pressure drop, alteration of particle morphology and rearrangement of the collected particles as a result of the formation of eutectic melts, and the filling of interparticle voids by the additional formation of sulfate salts on the surfaces of incompletely reacted sorbent particles.

Because the relationships between chemical constituents and particulate behavior are not yet established for gasification processes, the effect on filtration behavior of the various chemical compounds present in gasification particulate samples are not yet known. Chemical reactions such as tar formation and chemical sintering between particles have the potential to create problems such as bridging in filters collecting gasification particulates.

Some of the gasification chars studied under this task comprised irregularly-shaped particles with very high specific surface areas, and often exhibited extremely fine size distributions. Chars with very high surface areas ($> 100 \text{ m}^2/\text{g}$) have the potential to generate filter cakes that have extremely low permeabilities. In addition, there is a potential for some filter cakes comprising gasifier char to compact, which would adversely affect permeability. Also, many of the gasification char samples studied under this task exhibited relatively low tensile strengths. The low tensile strengths measured for these samples may indicate that char particles dislodged from filter elements during pulse cleaning cycles may break up into very small agglomerates. If this type of breakup occurs, reentrainment of previously collected gasification residues may pose a significant problem. Continued observation of the behavior of gasifier char filter cakes in HGCU filters is needed to assess to what extent these phenomena (the formation of low permeability filter cakes, filter cake compaction, and particle reentrainment) occur.

This task has catalogued many characteristics of PFBC ashes and gasification chars, and has studied the fundamental ways in which these characteristics ultimately affect filter operation. Figure 1-1 summarizes the ranges measured for some of the key physical characteristics of the filter cake samples discussed in this report. As can be seen in this figure, there are several distinct differences between these two types of filter cake material. This report examines these data in detail, and discusses the implications of these characteristics on HGCU filter performance. In addition to this report, the interactive data bank issued as a deliverable to DOE/FETC under this task serves as an important tool for advancing these studies. (The reader of this report is referred to the DOE/FETC Project Manager, Thomas P. Dorchak, for access to the interactive data bank.)

In order to maximize the benefit of the characterization and analysis of particulate properties for HGCU technology, additional samples should be analyzed as they become available, operating data and observations from operating HGCU facilities should continue to be compiled, and critical analysis of these data must continue to be performed and communicated to the users of these filters. Tasks like the one described in this report, and especially the interactive data bank it produced, provide excellent means for achieving these continuing objectives.

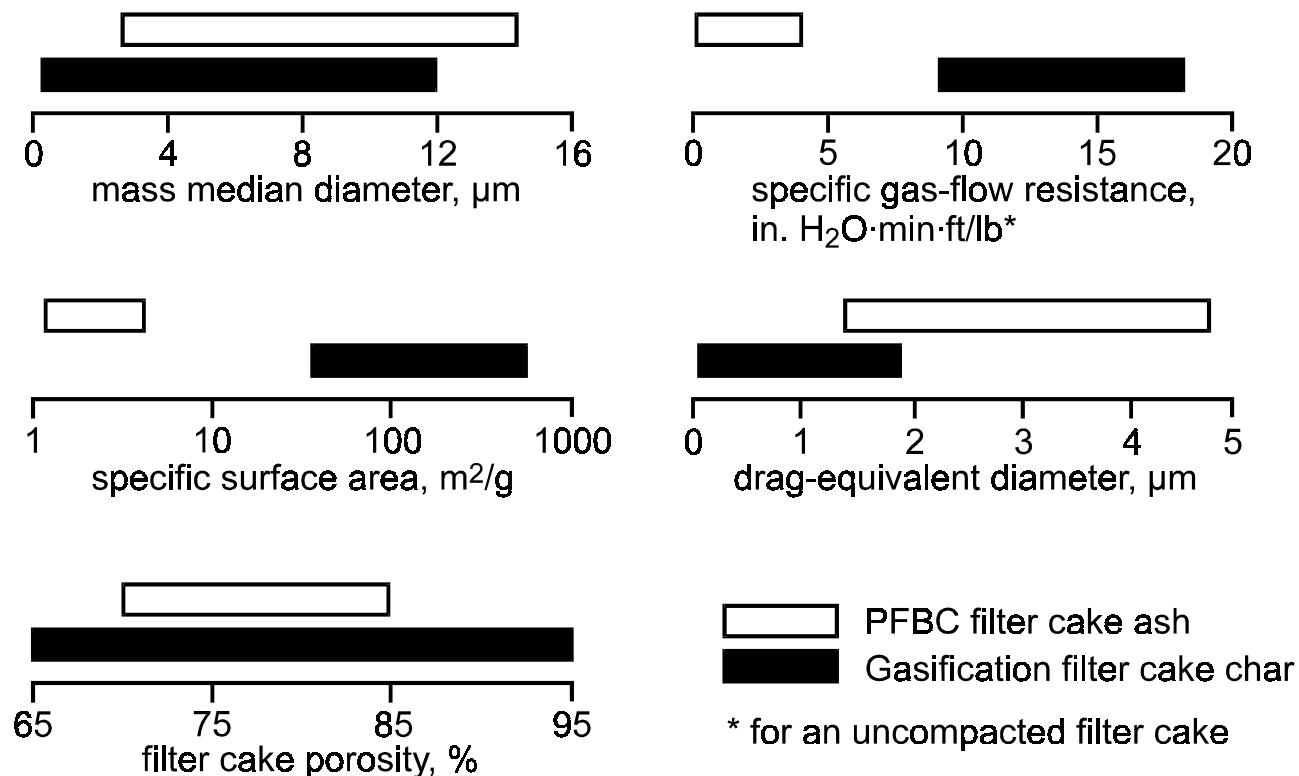


Figure 1-1. Ranges measured for some of the key physical characteristics of the filter cake samples discussed in this report.

2.0 INTRODUCTION

This is the final technical report describing the activities performed under Contract No. DE-AC21-94MC31160. Task 1 of this contract concerned analyses of HGCU ashes and descriptions of filter performance that were designed to address problems with filter operation linked to characteristics of the collected particulate matter. Much of the work conducted under Task 1 built directly on work performed under a prior contract (No. DE-AC21-89MC26239) with the Department of Energy's Federal Energy Technology Center in Morgantown, WV (DOE/FETC-MGN). Discussions of Task 2 of this contract are presented under separate cover, and concern characterization of new and used filter elements. Some of the problems observed at PFBC facilities include excessive filtering pressure drop, the formation of large, tenacious ash deposits within the filter vessel, and bent or broken candle filter elements. These problems have been attributed to ash characteristics, durability of the ceramic filter elements, and specific limitations of the filter design. In addition to the problems related to the characteristics of PFBC ashes, laboratory characterizations of gasifier and carbonizer particulates have shown that they also have characteristics that might negatively affect filtration. Specifically, gasifier particulates form filter cakes that could accumulate in thickness quite rapidly, might compact as a result of the filtering pressure drop across them, and also may tend to reentrain following cleaning pulses.

To identify which particulate characteristics can lead to problems with filtration, 375 particulate samples from fourteen facilities involved in FETC's HGCU program have been assembled into an interactive, computerized data bank. Three samples from gasification studies carried out by Herman Research Pty Ltd. (HRL) of Melbourne, Australia have also been studied under this task and are included in the data bank. An overview of these facilities and samples is provided in Table 2-1. Many of the samples have been analyzed with a variety of laboratory tests. Physical attributes of the particles that have been examined include size distribution, specific surface area, particle morphology, and bulk ash cohesivity and permeability. A range of chemical analyses of these samples, as well as characterizations of agglomerates of particles removed from filter vessels at Tidd, Karhula, the Power Systems Development Facility, and Foster Wheeler's pilot-scale combustion facility located in Livingston, New Jersey have also been performed. The data obtained in these studies were assembled into an interactive, computerized data bank to help the manufacturers and operators of high-temperature barrier filters tailor their designs and operations to the specific characteristics of the particulate materials to be collected. This report describes the methods used to analyze the HGCU particulate samples, presents the data measured for these samples, and discusses the implications these data have for HGCU filter operation at PFBC and gasification facilities.

2.1 OBJECTIVES

Task 1 had two primary objectives. The first was to generate a readily accessible data bank of the key characteristics of particulate samples collected from operating advanced particle filters. The second objective was to relate these measured properties and the contents of the data bank to the operation and performance of the advanced particle filters and filter components. The first objective included formatting the data bank and collecting, analyzing, and maintaining particulate samples from operating HGCU facilities. The second objective

of this task involved the collection of operating histories from advanced particle filters, correlating these histories with sample characteristics, interpreting these correlations, and communicating results in the various venues prescribed by DOE/FETC-MGN.

Table 2-1
Overview of Facilities and Particulate Samples

# of samples	HGCU facility	Process
7	New York University	bubbling bed PFBC
8	Kellogg Brown & Root	circulating PFBC
14	Kellogg Brown & Root	gasification
2	Texaco Montebello Research Lab	gasification
11	Grimethorpe	circulating PFBC
9	KRW	gasification
2	Allison	coal-fired combustion turbine
10	Foster Wheeler	carbonizer
7	Foster Wheeler	circulating PFBC
3	Iowa State University	AFBC
61	Karhula	circulating PFBC
116	Tidd	bubbling bed PFBC
12	DOE/FETC	gasification
7	UNDEERC transport reactor	gasification
2	UNDEERC transport reactor	circulating PFBC
3	Herman Research Pty Ltd.	gasification
101	PSDF transport reactor	circulating PFBC
3	Piñon Pine Power Project	gasification

3.0 FIELD SAMPLING AND ON-SITE MEASUREMENTS

Site visits were made to three HGCU filters which included observations, on-site measurements, documentation of the condition of the filter, and collection of samples for analysis. Descriptions of the conditions of these filters during each of these visits are presented in this section, along with brief descriptions of the HGCU facility visited. (Descriptions of the other HGCU facilities from which particulate samples were received for analysis under this task are presented under section 4.0 *Analyses of Particulate Samples*.)

Each site visit conducted under this task began with photographic documentation of the condition of the filter vessel. The ranges of on-site measurements and samples that can be obtained during site visits depend on the types of particulate deposits in the vessel, the condition of the filter elements, and the constraints of the sampling location. During several of these visits, areal density determinations and cake thickness measurements were made at various locations on the surfaces of the filter elements. (When both of these measurements can be made close to one another, filter cake porosity can be calculated.) These measurement techniques, which are described below, were limited to elements located on the outer perimeter of the filter arrays.

The measurement of areal density is made with a thin-walled core sampling tube that has a leading edge shaped to conform to the outer surface of the cylindrical filter elements. After a representative region is selected for this measurement, the sampling tube is pressed laterally through the filter cake until it firmly and evenly contacts the surface of the filter element. While it is held in place, the filter cake adjacent to the area isolated within the tube is brushed away to expose the surface of the filter element. A small catch basin shaped to conform to the outer surface of the filter element is placed below the core sampling tube, and the tube is gently removed so that any particulate material falling out of the tube is caught in the basin. Once the sampling tube has cleared the surface of the cake, its contents are added to any material already in the basin. Finally, the filter cake adhered to the surface of the element is brushed into the catch basin. The areal density of the sampled region is calculated by dividing the weight of the material collected by the cross-sectional area of the sampling tube.

A traversing transverse laser gauge is used to measure the thickness of filter cakes. After a region of the filter cake is selected, the gauge, which is mounted on a tripod, is positioned so that the horizontally-directed laser beam is tangent to the curvature of the filter element for the region of interest. The laser is mounted on a linear traversing mechanism so the beam can be moved horizontally at a right angle to its direction. The traversing mechanism includes a scale to record the location of the beam. Two positions of the beam are needed for a thickness measurement. The first is when the beam just contacts the surface of the filter cake. After this position is recorded, the filter cake between the contact point of the beam with the cake and the element surface is brushed away to expose the surface of the filter element. Then the beam is traversed laterally until it just contacts the surface of the cleaned region of the filter element. This second position is recorded, and the thickness of the cake is the difference between these two readings.

Other measurement and sample preservation techniques that have been made on site include preservation of nodules and deposits with epoxy (described under *Nodule Porosity* in section 4.1 *Laboratory Methods Used to Characterize Samples*), and preservation of the filter cakes on the surface of a candle removed from the filter vessel to an on-site laboratory. This technique is described in *Appendix A Technique for Preserving Filter Cakes*.

3.1 TIDD

The objective of the test program carried out at Tidd was to evaluate the design and obtain operating experience for a commercial size Advanced Particle Filter (APF) through long-term testing on a slipstream at Ohio Power Company's Pressurized Fluidized Bed Combustion (PFBC) Demonstration Plant. The 70 MWe Tidd PFBC Demonstration Plant in Brilliant, Ohio was completed in late 1990, and operated through March 1995 as part of the Department of Energy's Clean Coal Technology Program. The original design of the Tidd Plant utilized seven strings of primary and secondary cyclones to remove 98% of the particulate matter from the gases between the fluidized bed and the gas turbine. A HGCU slipstream replaced one of the seven secondary cyclones by taking the discharge gas of one of the primary cyclones to outside of the combustor vessel and into the APF.¹ The general features of the APF are shown in Figure 3-1. The filter was designed to operate with 384 filter elements, each nominally 2.36 in. (6 cm) O.D. and 4.92 feet (150 cm) long.⁸

Under the original maximum design load conditions, gas at approximately 150 psig, 1550 °F flowed into the filter at 7600 acfm with a dust loading of 600 ppmw. In January 1994, the dust loading was increased to 3400 ppmw by detuning the primary cyclone upstream of the APF. During the tests conducted in 1994, the APF generally operated between 1350 and 1450°F. In January 1995, the primary cyclone was bypassed which increased the loading to approximately 20,000 ppmw. This change was made to take advantage of a larger particle size distribution, as described later in this section. The operating temperature of the APF was allowed to reach 1550 °F for a significant portion of its operation with the cyclone bypassed.¹

Southern Research Institute personnel made four site visits to the Tidd APF to inspect and document the condition of the filter vessel and to collect for analysis representative samples of the various deposits of ash found in the APF. The first two of these visits were made on an earlier contract (No. DE-AC21-89MC26239). All four site visits are discussed in this section. In addition, a topical report entitled *Analyses of Ashes from the Tidd PFBC Advanced Particulate Filter* summarizing on-site observations and the results of on-site and laboratory ash analyses was submitted in August 1995 to DOE/FETC-MGN.

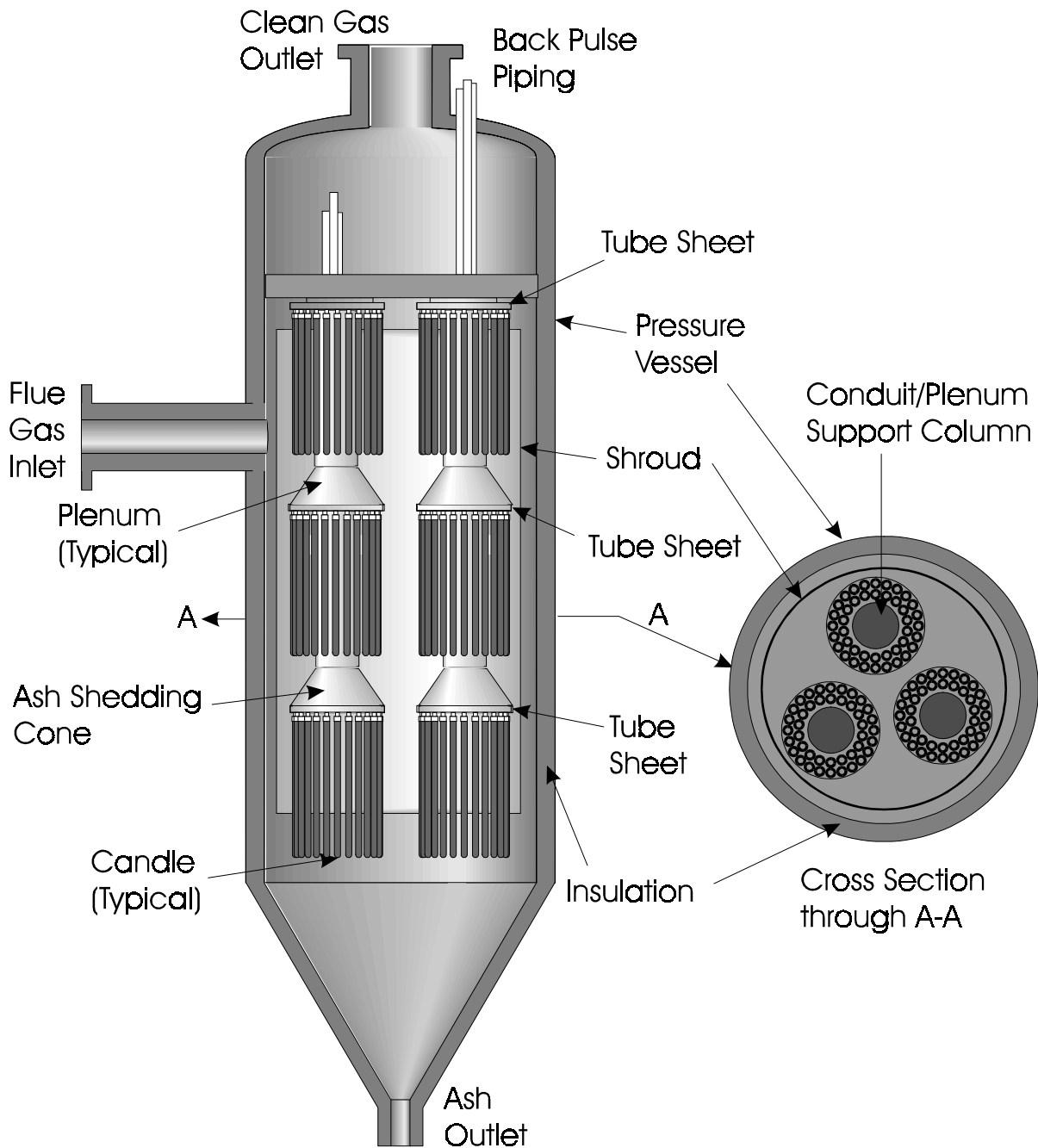


Figure 3-1. General features of the APF at the Tidd Demonstration Plant.

3.1.1 September 30, 1993

When the filter assembly was opened on September 30, 1993, extensive deposits of ash were found on candle surfaces, bridged between candles, and on non-filtering surfaces (ash sheds, plenum support conduits, and on the underside of the tube sheet). Deposits found on these non-filtering surfaces were formed by the gradual deposition of particles as a result of turbulent diffusion. Some of these passive deposits were up to six inches thick, with high

tensile strength. Many of the candle filter elements were covered by filter cakes up to one inch thick. Like the passively deposited agglomerates of ash, these filter cakes also had high tensile strength. Figures 3-2 through 3-5 provide representative views of the condition of the APF as observed on this site visit. Figure 3-6 shows one of the thick, strong filter cake specimens collected while on site.



Figure 3-2. Severe ash bridging was evident as the top two plenums were lifted into view.



Figure 3-3. Thick, patchy cakes were present throughout the filter vessel.



Figure 3-4. Ash almost completely enveloped many of the candle filter elements.



Figure 3-5. The appearance of these candles is believed to be the result of patchy cleaning and the loss of cake during cooling down of the filter vessel.



Figure 3-6. A number of laboratory analyses were performed on this thick filter cake deposit (ID # 4012). The deposition layers formed during filtration are clearly visible in this specimen.

3.1.2 May 5, 1994

The filter vessel was again opened for inspection and refitting on May 5, 1994. Despite the relative cleanliness of the candles, significant deposits of ash were observed at several other locations in the assembly. The undersides of all of the nine tube sheets were coated with deposits of ash about eight inches thick. Although the outer (presumably the most recently deposited) portions of these deposits were fairly fluffy, the inner regions were hard, strong, and well consolidated. Similar deposits were found on the ash sheds above the middle and bottom plenums. These deposits were about three inches thick, and were also strong and well consolidated. Strong, thick deposits were present on the plenum support conduits positioned in the center of the top and middle plenum assemblies. These deposits were thick enough (over four inches) in most areas to envelop the inner ring of candles in these plenum assemblies. Many of the innermost candles in the top and middle plenums were bent away from the plenum support conduits. The regions between these candles and the plenum support conduits were almost completely filled with ash. Figures 3-7 through 3-23 document the condition of the APF on this site visit.

Observations of the APF during this site visit indicated that severe bridging of ash between adjacent candles was still a serious problem. Many ash bridges were present, some of which extended from the deposit on the underside of the tube sheet all the way down to the conical surface of the ash shed below the bottom ends of the candles. Ash bridges were identified in many different stages of formation. Most ash bridges were found in the top and middle plenums, which were also the locations where most of the severely bent candles were found. The bottom plenums had the fewest ash bridges, and the fewest bent or broken candles. As was observed previously, the ash deposits throughout the APF had high tensile strength. However, the filter cakes observed during this second site visit were only about 0.4 inch thick, compared with the one-inch thick cakes present in September 1993.